Theor Chem Acc (1999) 102:165–169
DOI 10.1007/s002149800m80

Theoretical
Chemistry Accounts

Regular article

RISM-SCF study of the free-energy profile of the Menshutkin-type reaction $NH_3 + CH_3Cl \rightarrow NH_3CH_3^+ + Cl^-$ in aqueous solution*

Kazunari Naka[1], **Hirofumi Sato**[2], **Akihiro Morita**[1], **Fumio Hirata**[2], **Shigeki Kato**[1]

[1] Department of Chemistry, Graduate School of Science, Kyoto University, Kitashirakawa, Sakyo-ku, Kyoto 606-8502, Japan
[2] Institute for Molecular Science, Myodaiji, Okazaki, Aichi 444-8585, Japan

Received: 26 June 1998 /Accepted: 28 August 1998 / Published online: 2 November 1998

Abstract. The free-energy profile for the Menshutkin-type reaction $NH_3 + CH_3Cl \rightarrow NH_3CH_3^+ + Cl^-$ in aqueous solution is studied using the RISM-SCF method. The effect of electron correlation on the free-energy profile is estimated by the RISM-MP2 method at the HF optimized geometries along the reaction coordinate. Solvation was found to have a large influence on the vibrational frequencies at the reactant, transition state and product; these vibrational frequencies are utilized to calculate the zero-point energy correction of the free-energy profile. The computed barrier height and reaction exothermicity are in reasonable agreement with those of experiment and previous calculations. The change of solvation structure along the reaction path is represented by radial distribution functions between solute-solvent atomic sites. The mechanisms of the reaction are discussed from the view points of solute electronic and solvation structures.

Key words: Menshutkin reaction – Solvation effect – RISM-SCF

1 Introduction

Electronic structure calculations for free-energy surfaces of chemical reactions in solution have received much attention in recent years. Various methods taking account of solvent effects in solute electronic structure calculations have been proposed. The most popular approach has regarded the solvent as a macroscopic continuum medium characterized by the dielectric constant [1]. Several models have been developed within the framework of the dielectric continuum approximation and have been successfully applied to many molecular processes in solution. It is noted, however, that these approaches do not provide any information about solvation structures at the microscopic level and are not capable of describing a local solute–solvent interaction such as hydrogen bonding. There is also ambiguity in defining the shape and size of the solvent cavity inherent in these methods.

The hybrid quantum mechanical/molecular mechanics (QM/MM) method [2], on the other hand, treats solvent molecules explicitly, and therefore provides detailed information of solvation structures. Although the QM/MM method has an advantage in treating intermolecular interaction explicitly at a molecular level, it is computationally too demanding to carry out calculations of free-energy surfaces of complex chemical reactions, because large-scale simulation calculations such as Monte Carlo or molecular dynamics for a large number of solvent molecules are required to obtain converged results for the free energy.

The reference interaction site model self-consistent-field (RISM-SCF) method [3] is regarded as an intermediate between the dielectric continuum and QM/MM approaches. This method incorporates the molecular aspects of the solvent through the solvent distribution functions obtained by the integral equation based on the RISM for polyatomic liquids. Using this method, one can determine the solute electronic and solvation structures in a self consistent manner with reasonable computational cost.

In the present paper, we have applied the RISM-SCF method to calculate the free-energy profile of the Menshutkin-type S_N2 reaction [4] in aqueous solution

$$NH_3 + CH_3Cl \rightarrow NH_3CH_3^+ + Cl^- \quad .$$

This reaction has been studied by the various methods mentioned above. Gao [5] and Gao and Xia [6] performed QM/MM simulations to obtain the free-energy surface and provided an interpretation for the exothermicity of the reaction and the transition state (TS) shift in aqueous solution by considering microscopic solvation structures. This pioneering work was followed by several dielectric continuum approaches. Dillet et al. [7] developed the multipole expansion

*Contribution to the Kenichi Fukui Memorial Issue
Correspondence to: K. Naka

technique to solve the Poisson-Laplace equation in the dielectric continuum model and applied it to explore the free-energy profiles in various solvents. The generalized conductor-like screening model [8] was employed by Truong et al. [9] combining it with second-order Møller-Plessset perturbation (MP2) and density functional theories. The polarizable continuum model (PCM) [10] was employed by Fradera et al. [11] to analyze the solution phase potential energy surface. Very recently, Amovilli et al. [12] studied the free-energy profiles using the complete active space SCF method combined with the PCM.

Considering these circumstances, it would be meaningful to apply the RISM-SCF method to the same reaction. The purposes of the present paper are (1) to compare the RISM-SCF free-energy profile with those obtained by the other methods, and (2) to provide information on solvation structures for use in interpreting the solvation effects on the reaction mechanism. We also examined the effect of electron correlation on the free-energy profile. The organization of the paper is as follows. In Sect. 2, the theoretical methods employed in the present calculations are described. We show the calculated results in Sect. 3 and these are compared with previous calculations based on various theoretical models. The conclusions are summarized in Sect. 4.

2 Method

The free-energy profile in aqueous solution was calculated by the RISM-Hartree-Fock (HF) method, where the HF wavefunction was used to describe the electronic structures of the solute. The reaction coordinate was taken to be the difference of the C—Cl and C—N distances as shown in Fig. 1. The solute geometry along the reaction path was determined by optimizing the other internal degrees of freedom while maintaining C_{3v} symmetry at each value of the reaction coordinate. We used the energy gradient technique for the RISM-HF free energy [13]. We also obtained the harmonic vibrational frequencies at the optimized geometries for reactants, TS and product. The hessian matrices were derived by numerical differentiation of analytically calculated energy gradients. We used the $(9s5p1d/4s1p)/[3s2p1d/2s1p]$ basis set [14], which has a double zeta plus polarization (DZP) quality, for C, N and H atoms. For Cl, the $(11s7p1d)/[6s4p1d]$ DZP basis set augmented with a diffuse p-function with the exponent 0.049 was used [14], since the diffuse function is necessary to describe Cl^- at the product region.

The simple point-charge like model [15] was employed for solvent water molecules. For the solute, the Lennard-Jones parameters were chosen from AMBER [16] for C,N and H atoms, while those of Cl were from Ref. [6]. We applied the standard combination rule to construct the solute-solvent van der Waals interactions. The solute partial charges were determined by least-square fitting to the electrostatic potential. The grid points utilized in the fitting procedure were generated around the solute atoms based on Voronoi polyhedrons [17] and the number of grid points was about 2500. In solving the RISM integral equation, the hyper-netted-chain (HNC) closure relation was employed under the conditions that the temperature was 298.15 K and the density of solvent was 0.033329 molecule $Å^{-3}$, respectively. The solvation free energy was also estimated with the Gaussian fluctuation (GF) approximation [18], where the solute-solvent correlation functions obtained with the HNC closure were used.

In order to examine the effect of electron correlation on the reaction free-energy profile, we also carried out RISM-MP2 calculations at the RISM-HF optimized geometries along the reaction coordinates. It is noted that the MP2 energy for RISM-HF is given in a slightly different form from the usual one in the gas phase. In the case of RISM-HF, the second-order correlation energy is estimated by

$$E^{(2)} = \frac{1}{4}\sum_{abrs}\frac{|<ab||rs>|^2}{\varepsilon_a + \varepsilon_b - \varepsilon_r - \varepsilon_s} \quad ,$$

where a and b denote an occupied orbital pair, and r and s unoccupied orbitals, respectively. The orbital energy ε is defined in terms of the solvated Fock operator [3]. This equation is easily derived with the consideration that the electrostatic potential from the solvent is the one-electron operator and does not appear in the numerator.

3 Results and discussion

3.1 Free-energy profile

The free-energy profiles along the reaction coordinate calculated both by the RISM-HF and the MP2 method are shown in Fig. 2. Although this reaction is endothermic in the gas phase by 106.3 kcal/mol with the HF method, it becomes exothermic in aqueous solution by 27.8 kcal/mol at the RISM-HF level. The barrier height was calculated to be 17.7 kcal/mol. As seen in Fig. 2, there is a shallow potential well around 1.9 Å, which corresponds to a contact ion-pair of $NH_3CH_3^+$ and Cl^- formed in aqueous solution.

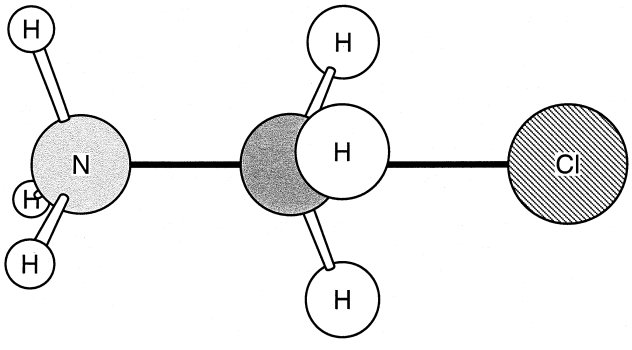

Fig. 1. Geometry of the reaction system. The reaction coordinate was taken to be the difference of the C—Cl and C—N distances

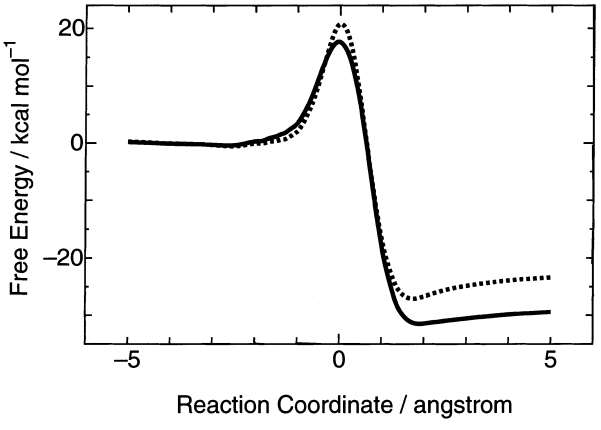

Fig. 2. Reaction free-energy profile. *Solid* and *dotted lines* are for HF and MP2 calculations, respectively

Table 1. Optimized geometries (distances in Å, angles in degrees) and solvation free energy (kcal/mol) for the reactants, products and transition state for the reaction in aqueous solution

Parameter	Solution	Gas
	NH_3	
NH	1.005	1.002
∠HNH	106.8	107.9
ΔG_{hyd}(HNC)[a]	−8.0 (−4.3)[b]	
ΔG_{hyd}(GF)[c]	−15.0	
	CH_3Cl	
CCl	1.799	1.788
CH	1.076	1.078
∠HCCl	107.6	108.2
ΔG_{hyd}(HNC)[a]	13.2 (−0.6)[b]	
ΔG_{hyd}(GF)[c]	2.2	
	$H_3NCH_3^+$	
CN	1.490	1.507
NH	1.013	1.010
CH	1.076	1.078
∠HNC	111.9	111.4
∠HCN	108.5	108.2
ΔG_{hyd}(HNC)[a]	−49.2 (−70)[b]	
ΔG_{hyd}(GF)[c]	−59.4	
	Cl^-	
ΔG_{hyd}(HNC)[a]	−81.5 (−77)[b]	
ΔG_{hyd}(GF)[c]	−87.8	
	TS	
CN	2.258	1.890
CCl	2.258	2.490
CH	1.066	1.066
NH	1.006	1.004
∠HNC	111.7	110.7
∠HCN	87.3	96.8

[a] Hyper-netted-chain (HNC) closure relation
[b] The values in parentheses are from Ref. [12]
[c] Gaussian fluctuation (GF) approximation

The optimized geometry of the TS is given in Table 1 along with those of the reactant and product. We also included the geometries of the stationary points in the gas-phase reaction for comparison. In solution, the reactants, NH_3 and CH_3Cl deform so as to increase the dipole moments; the CCl distance increases by 0.01 Å and the HNH angle in NH_3 and the HCH angle in CH_3Cl decrease by 1.1 and 0.6°, respectively. The geometrical change for the product $NH_3CH_3^+$ occurs so as to localize the positive charge, in agreement with the result of Truong et al. [9]. Compared to the gas-phase case, the location of the TS shifts toward the reactant side in aqueous solution; the CN and CCl distances are almost the same, 2.258 Å, while those in the gas phase are 1.890 and 2.490 Å, respectively, and the CNH angle is reduced by 9.5°. This is consistent with Hammond's postulate [19] for the TS location and the results of previous calculations.

The MP2 calculations provided a rather sharper free-energy curve near the TS and the barrier height was calculated to be 20.9 kcal/mol, which is higher than the HF value by 3.2 kcal/mol. The reaction exothermicity is reduced by 5.7 kcal/mol with MP2, and thus became 22.1 kcal/mol. It is noted that the MP2 TS is located at almost the same position as that of the HF calculation.

Table 2. Harmonic frequencies (cm^{-1}) for the reactants, transition state and products in aqueous solution and in the gas phase

	Solution	Gas	Description
NH_3	1100	1132	NH_3 umbrella
	1716	1806	NH_3 deformation[a]
	3682	3720	N—H stretch
	3808	3864	N—H stretch[a]
TS	589i	550i	Asymmetric stretch
	126	195	NH_3, CH_3 rotation[b]
	170	199	NCCl bend
	237	270	Symmetric stretch
	428	698	NH_3, CH_3 rock[a,b]
	1003	1169	CH_3 rock[a]
	1122	1312	CH_3 umbrella, asymmetric stretch
	1263	1387	NH_3 umbrella
	1471	1531	CH_3 deformation[a]
	1665	1798	NH_3 deformation[a]
	3366	3369	C—H stretch
	3580	3574	C—H stretch[a]
	3675	3699	N—H stretch
	3806	3840	N—H stretch[a]
	3806	3840	N—H stretch
$H_3NCH_3^+$	313	305	NH_3, CH_3 rotation[b]
	983	974	NH_3, CH_3 rock[a]
	1041	987	C—N stretch
	1379	1383	NH_3, CH_3 rock[a]
	1524	1585	CH_3 umbrella
	1609	1672	NH_3 umbrella
	1640	1621	CH_3 deformation[a]
	1702	1802	NH_3 deformation[a]
	3286	3271	C—H stretch
	3401	3391	C—H stretch[a]
	3609	3650	N—H stretch
	3693	3755	N—H stretch[a]
CH_3Cl	746	785	C—Cl stretch
	1120	1122	CH_3 rock[a]
	1499	1515	CH_3 umbrella
	1541	1609	CH_3 deformation[a]
	3271	3260	C—H stretch
	3395	3374	C—H stretch[a]

[a] Degenerate mode
[b] These modes are mixed

The vibrational harmonic frequencies of reactant, TS and product in solution are compared with those in the gas phase in Table 2. The frequencies of the NH stretching modes decrease by 20–60 cm^{-1} in solution, reflecting the fact that hydrogen bonds are formed between the H atoms in NH_3 and O in H_2O. On the other hand, the frequencies of the CH stretching modes slightly increase due to hydrophobic interaction with the water solvent. For the bending vibrations, both the deformation and umbrella modes of NH_3 and CH_3 are softened by solvation, except for the CH_3 deformation in the product.

At the TS, the vibrational frequencies of all the modes except for the degenerate CH stretching are smaller than those at the gas-phase TS. The CH_3 umbrella frequency (1122 cm^{-1}) is considerably reduced compared with those of reactant (1499 cm^{-1}) and product (1523 cm^{-1}), indicating that Walden inversion facilitates the reaction. After including the zero-point energy corrections, the barrier height and reaction exo-

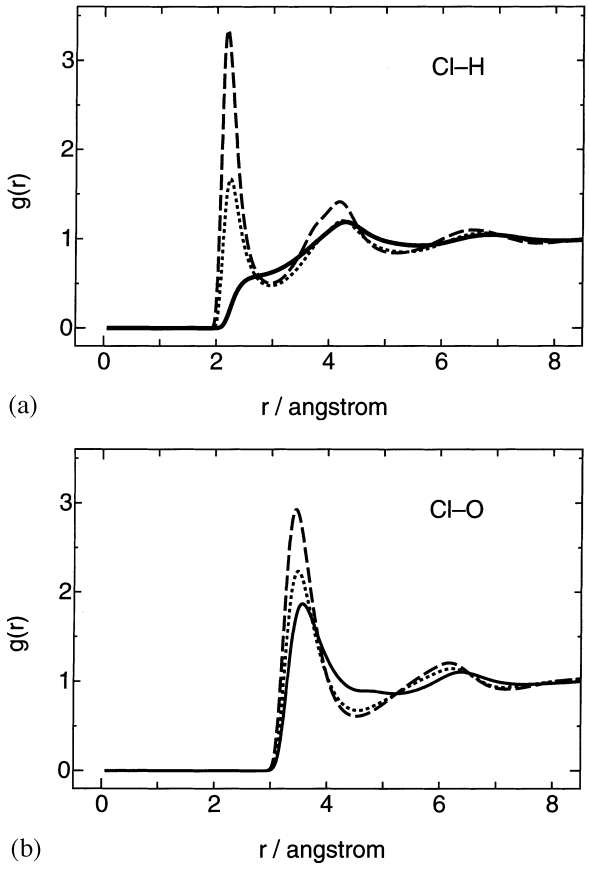

Fig. 3a,b. Site-site pair distribution functions between the solute Cl and H_2O. *Solid*, *dotted* and *dashed lines* correspond to the reactants, transition state and products, respectively

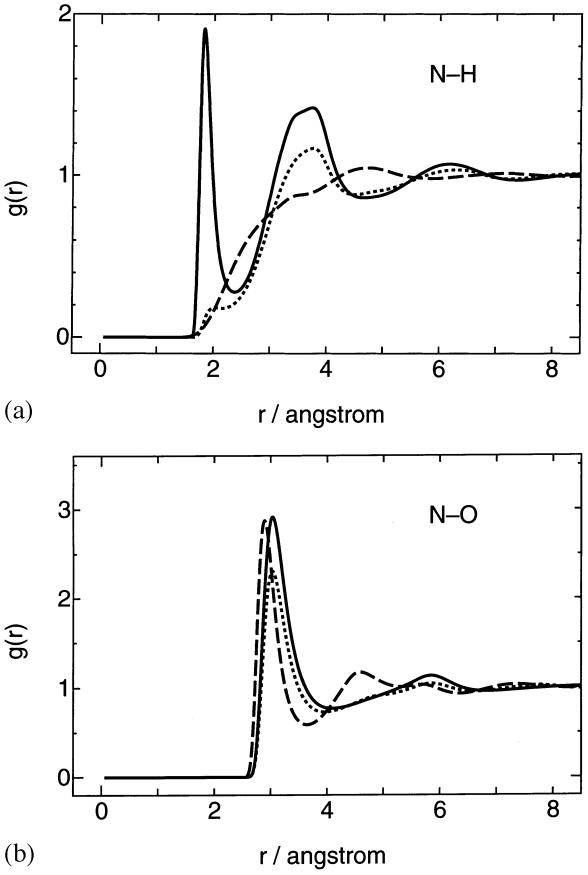

Fig. 4a,b. Site-site pair distribution functions between the solute N and H_2O. *Solid, dotted* and *dashed lines* correspond to the reactants, transition state and products, respectively

thermicity thus became 21.7 and 17.1 kcal/mol, respectively.

Theoretical values of the barrier height and reaction exothermicity obtained with various methods have been reported in the literature [5–7, 9, 11, 12]. The potential barrier height reported so far lies in the range 16.8–31.4 kcal/mol. The present result, 21.7 kcal/mol, is in reasonable agreement with previous calculations. The calculated reaction exothermicity, 17.1 kcal/mol, seems too small compared with the experimental estimate, 34 ± 10 kcal/mol [20]. This is mainly attributed to discrepancies of solvation free energies of the reactant and product species, particularly for CH_3Cl and $NH_3CH_3^+$, as seen in Table 1, though these errors are largely canceled out between reactant and product. Also shown in Table 1 are the solvation free energies obtained with the GF approximation, which gave improved values for the solvation free energy. With the GF approximation, the barrier height and reaction exothermicity are estimated to be 20.6 and 21.9 kcal/mol, respectively.

3.2 Solvation structure

The radial distribution functions (RDFs) between the solute-solvent atomic sites are shown in Figs. 3 and 4, where the solid, dotted and dashed lines are for the reactant, TS and product, respectively. As seen in Fig. 3a, the Cl—H RDF clearly demonstrates the progress of hydrogen bonding along the reaction coordinate. At the reactant, the peak corresponding to the Cl—H interaction is not observed. The distinct first peak around $r = 2.2$ Å grows up monotonically and slightly shifts toward the inside as the reaction proceeds. The other H atom of H_2O in the first solvation shell corresponds to the second peak around 4.2 Å. The number of H_2O molecules hydrogen bonded to Cl was estimated by integrating the first peak of the RDFs and was found to be 4.3 and 6.6 at the TS and product, respectively, which is comparable to the QM/MM result, 3.1 and 6.6, respectively [6]. The Cl—O RDF in Fig. 3b has the first peak around 3.5 Å, and its height increases as the reaction proceeds. The smaller number of surrounding H_2O at the reactant is due to the CH_3 group in the reactant CH_3Cl preventing H_2O from coordinating to the Cl atom.

The breaking of the hydrogen bond between the ammonia N and water H atoms is observed in Fig. 4a, where the first peak around 2.0 Å in the reactant disappears as the reaction progresses. Although the lone-pair electron on the N atom forms hydrogen bonds with H_2O in the reactant region, it participates to form a new chemical bond with the C atom of CH_3Cl in the reaction process. As seen in the N—O RDF (Fig. 4b), the first

peak around 3.0 Å decreases with approach to the TS. This is because the approach of NH_3 to CH_3Cl excludes H_2O molecules in the region between the N and C atoms. After the TS, the N—O peak becomes higher and slightly shifts to the inside, indicating a strong interaction between $NH_3CH_3^+$ and solvent H_2O molecules. The second peak is observed at $r = 4.5$ Å for the product, which is attributed to H_2O molecules coodinating to the positively charged CH_3 group in the product.

The formation of a Cl—H hydrogen bond and the breaking of a N—H one are the key ingredients for interpreting the solvent effect on the reaction mechanism. The present results for the Cl—H and N—H RDFs clearly demonstrate the importance of these hydrogen bonds and are consistent with QM/MM calculations by Gao and Xia [6]. However, a remarkable difference is found in the Cl—O, N—O and C—O RDFs between the present RISM-SCF calculations and QM/MM ones. Although the first peaks for these RDFs are rather sharp at all stages of reaction and their positions do not change so much in the RISM-SCF calculations, the features of the QM/MM RDFs undergo considerable change along the reaction path; the first peaks, Cl—O and N—O RDFs, are the rather diffuse and shift toward the outside at the reactant and TS in the QM/MM calculations. These results indicate that the positions of O atoms in the surrounding H_2O molecules are mainly determined by the repulsive part of solute-solvent interaction potential and the change of electronic structure of solute is responsible for determining the orientation of the OH bond in solvent H_2O in the RISM-SCF calculations, while the positions of O atoms as well as H atoms are very sensitive to the change of charge distribution of the solute in the QM/MM calculations.

4 Conclusions

We have calculated the free-energy profile of the S_N2 Menshutkin-type reaction, $NH_3 + CH_3Cl \rightarrow NH_3CH_3^+ + Cl^-$, in aqueous solution by the RISM-SCF method. The effect electron correlation was taken into account by RISM-MP2.

The calculated barrier height and reaction exothermicity as well as the location of the TS were comparable to the results of previous calculations based on the dielectric continuum and QM/MM models.

The solvation effects on the reactant, TS and product vibrations revealed that hydrogen bonding reduces the vibrational frequencies of all the vibrational modes except for some modes of the CH_3 group, for which hydrophobic interaction plays an important role.

The solvation structures along the reaction coordinate were discussed in terms of the RDFs between the solute-solvent atomic sites. The importance of the formation of Cl—H hydrogen bonds and the breaking of N—H ones was demonstrated in characterizing the reaction mechanism as in the previous QM/MM calculations. It is noted, however, that there are large discrepancies in the C1—O and N—O RDFs between the RISM-SCF and QM/MM results.

In conclusion, it was shown that the RISM-SCF method is a powerful tool for studying the free-energy surfaces of complex chemical reactions in solution. In particular, the present method gives microscopic information of solvation along the reaction path with reasonable computational cost.

Acknowledgements. The numerical calculation was performed at the Computer Center of the Institute of Molecular Science (IMS) and on our own workstations. This work was supported by the Grant-in-Aid for Scientific Research from the Ministry of Education, Japan.

References

1. Cramer JC, Truhlar DG (1995) In: Lipkowitz KB, Boyd DB (eds) Reviews in computational chemistry, vol 6. VCH, New York, pp 1–72
2. Gao J (1995) In: Lipkowitz KB, Boyd DB (eds) Reviews in computational chemistry, vol 7. VCH, New York, pp 115–189
3. (a) Ten-no S, Hirata F, Kato S (1993) Chem Phys Lett 214: 391; (b) Ten-no S, Hirata F, Kato S (1994) J Chem Phys 100: 7443
4. Menshutkin NZ (1890) Phys Chem 5: 589
5. Gao J (1991) J Am Chem Soc 113: 7796
6. Gao J, Xia X (1993) J Am Chem Soc 115: 9667
7. Dillet V, Rinaldi D, Bertrán J, Rivail J-L (1996) J Chem Phys 104: 9437
8. (a) Truong TN, Stefanovich EV (1993) Chem Phys Lett 240: 253; (b) Stefanovich EV, Truong TN (1996) J Chem Phys 105: 2961
9. Truong TN, Truong TT, Stefanovich EV (1997) J Chem Phys 107: 1881
10. (a) Miertús S, Scrocco E, Tomasi J (1981) Chem Phys 55: 117; (b) Tomasi J, Persico M (1994) Chem Rev 94: 2027
11. Fradera X, Amat L, Torrent M, Mestres J, Constans P, Besalú E, Martí J, Simon S, Lobato M, Oliva JM, Luis JM, Andrés JL, Solà M, Carbó R, Duran M (1996) J Mol Struct (THEOCHEM) 371: 171
12. Amovilli C, Mennucci B, Floris FM (1998) J Phys Chem B 102: 3023
13. Sato H, Hirata F, Kato S (1996) J Chem Phys 105: 1546
14. Dunning THJ, Hay PJ (1997) In: Schaefer HF III (ed) Methods of electronic structure theory. Plenum, New York, pp 1
15. Berendsen HJC, Postma JPM, Gunstern WF, Hermas J (1981) In: Pullman B (ed) Intermolecular forces. Reidel, Dordrecht, pp 231
16. Cornell WD, Cieplak P, Bayly CI, Gould IR, Merz KM Jr, Ferguson DM, Spellmeyer DC, Fox T, Caldwell JW, Kollman PA (1995) J Am Chem Soc 117: 5179
17. Friesner RA (1988) J Phys Chem 92: 3091
18. Chandler D, Singh Y, Richardson DM (1984) J Chem Phys 81: 1975
19. (a) Hammond GS (1955) J Am Chem Soc 77: 334; (b) Leffler J.E. (1953) Science 117: 340
20. Okamoto K, Fukui S, Shingu H (1967) Bull Chem Soc Jpn 40: 1920